Liquid metal Taylor-Couette experiment on the magnetorotational instability

Thomas Gundrum[1*], Frank Stefani[1], Gunter Gerbeth[1], Jacek Szklarski[1], Günther Rüdiger[2], Rainer Hollerbach[3.]

[1] Forschungszentrum Dresden-Rossendorf, P.O. Box 510119, D-01314 Dresden, Germany, e-mail address: (*Corresponding author, e-mail: th.gundrum@fzd.de)

[2] Astrophysikalisches Institut Potsdam, An der Sternwarte 16, D-14482 Potsdam, Germany

[3] Department of Applied Mathematics, University of Leeds, Leeds, LS2 9JT, United Kingdom

The magnetorotational instability (MRI) plays an essential role in the formation of stars and black holes. By destabilizing hydrodynamically stable Keplerian flows, the MRI triggers turbulence and enables outward transport of angular momentum in accretion discs. We present the results of a liquid metal Taylor-Couette experiment under the influence of helical magnetic fields that show typical features of MRI at Reynolds numbers of the order 1000 and Hartmann numbers of the order 10. The paper focuses on noise reduction in the frequency domain and the wave number domain using standard FFT and shows some preliminary results of selected experiments.

Keywords: Liquid metal, GaInSn, MRI, helical magnetic field, ultrasonic measurement

1. INTRODUCTION

Magnetic fields play a double role in the cosmos: First, planetary, stellar and galactic fields are produced by the homogeneous dynamo effect in moving electrically conducting fluids. Second, magnetic fields can accelerate tremendously the formation of stars and black holes, by enabling outward transport of angular momentum in accretion disks by virtue of the so-called magnetorotational instability (MRI). This instability had been discovered as early as 1959, when Velikhov showed that a Taylor-Couette flow in its hydrodynamically stable regime (i.e. with outward increasing angular momentum) can be destabilized by an applied axial magnetic field [1]. But it was only in 1991 that the relevance of MRI for accretion disks in the vicinity of young stars and black holes was realized in a seminal paper by Balbus and Hawley [2].

The last decades have seen remarkable theoretical and computational progress in understanding the dynamo effect and the MRI. The hydromagnetic dynamo effect has even been verified experimentally in large-scale liquid sodium facilities in Riga, Karlsruhe, and Cadarache, and is presently studied in laboratories around the world [3]. In contrast, attempts to study the MRI in the laboratory have been less successful so far [4]. An MRI-like instability has been observed on the back-ground of a turbulent spherical Couette flow [5], but the genuine idea that MRI would destabilize a hydrodynamically stable flow was not realized in this experiment.

One of the basic problems for the experimental investigation of the "standard MRI", with only an axial magnetic field being externally applied, is the need for flows with large magnetic Reynolds numbers ($R_m = \mu_0 \, \sigma \, v \, L \geq 1$, thereby μ_0 is the permeability of free space, σ the conductivity of the fluid, v its typical velocity, and L is the typical length scale of the flow).

The crucial point is that the azimuthal field, which is an essential ingredient of the MRI mechanism, must be produced from the applied axial field by induction effects proportional to the magnetic Reynolds number Rm. The natural question, why not substitute the induction process by externally applying the azimuthal field as well, was addressed by Hollerbach and Rüdiger [6]. It turned out that the scaling properties for this "helical MRI" are much more comfortable for building laboratory experiments than those of "standard MRI".

In this paper, we present preliminary results of the PROMISE 2 (**P**otsdam **RO**ssendorf **M**agnetic **InS**tability **E**xperiment) experiment. Results of PROMISE 1 were already published in [7-9].

2. THE EXPERIMENTAL FACILITY

The basic part of PROMISE 2 is a cylindrical containment vessel V made of copper cylinders (see fig. 1a). The inner wall of the vessel V is 10 mm thick, and extends in radius from 22 to 32 mm; the outer wall is 15 mm thick, extending from 80 to 95 mm. This vessel is filled with the eutectic alloy $Ga^{67}In^{20.5}Sn^{12.5}$ which is liquid at room temperatures. The vessel V, made of copper cylinders is fixed via a spacer D on a precision turntable T. The outer copper cylinder of the vessel represents the outer cylinder of the Taylor-Couette cell. The inner copper cylinder I of the Taylor-Couette cell is fixed to an upper turntable, and is immersed into the liquid metal from above. It has a thickness of 4 mm,

extending in radius from 36 to 40 mm, thus leaving a gap of 4 mm between this immersed cylinder I and the inner wall of the containment vessel V. The actual Taylor-Couette cell extends in radial direction over a cylindrical gap of width $d = r_{out} - r_{in} = 40\,mm$, and in axial direction over the liquid metal height of $z = 400\,mm$, resulting in an aspect ratio of 10.
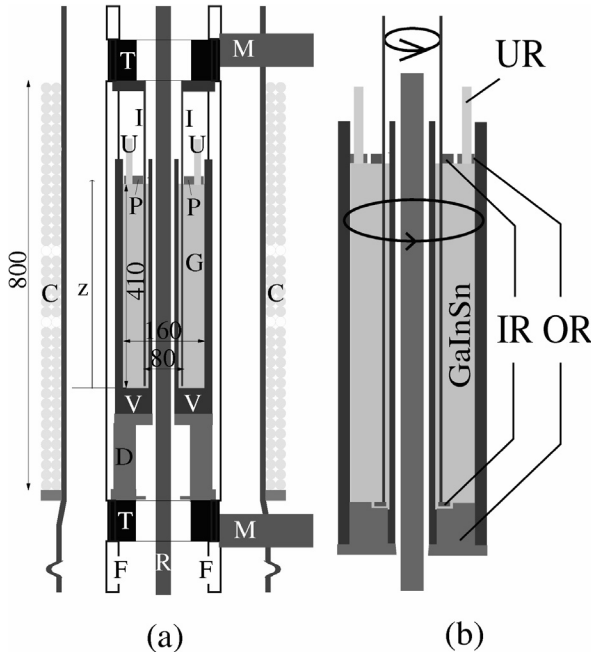
Figure 1. The PROMISE 2 experiment. (a) Sketch. (b) Taylor-Couette cell configuration. V - vessel, OR – Outer cylinder, I /IR – Inner cylinder, G – GaInSn, U/UR – Rotating ultrasonic transducers, P – Plexiglas lid, T - High precision turntables, M – Motors, F - Frame, R – Copper rod for azimuthal field, C – Coil for axial field. The indicated dimensions are in mm.

Figure 1b shows the PROMISE 2 symmetric end cap configuration: Both end caps are made of insulating material in order to avoid short-circuiting of currents along the copper end cap at the bottom. The upper and the lower end caps are split into two rings, the inner rings rotate with the inner cylinder and the outer rings rotate with the outer cylinder. In [10] it had been shown that this splitting yields a minimization of the Ekman pumping if the position of the splitting is at 0.4 of the gap width d. The co-rotation of the two rings with one of the cylinders made it necessary to guide the signal transmission of the ultrasonic transducers via an sliding contact below the vessel. These two transducers provide full profiles of axial velocity v_z along the beam-lines. Data acquisition was carried out with Ultrasonic Doppler Velocimeter (DOP 2000).

An axial magnetic field of order 10 mT is applied by a double-layer coil (C in fig. 1). The coil is fed by currents up to 200 A. The azimuthal field, also of order 10 mT, is generated by a current through a water-cooled copper rod R of radius 15 mm. The

power supply for this axial current is capable of delivering up to 8000 A.

3. DATA PROCESSING

The ultrasonic transducers UR in figure 1b are fixed at the outer ring at $r_{UR} = 68\,mm$ and shifted by $180°$ to each other. This configuration was chosen in order to eliminate non-axisymmetric velocity structure. This unwanted velocity structure superimposes the desired MRI signal. Figure 2 shows the time dependent signal of one transducer. The grey scale of the plot represents the axial velocity v_z, from which the z-dependent time average velocity va, plotted on the right hand side of figure 2, was subtracted in order to filter out the two Ekman vortices. These Ekman vortices are characterized by inward radial flows close to the upper and lower endplates.
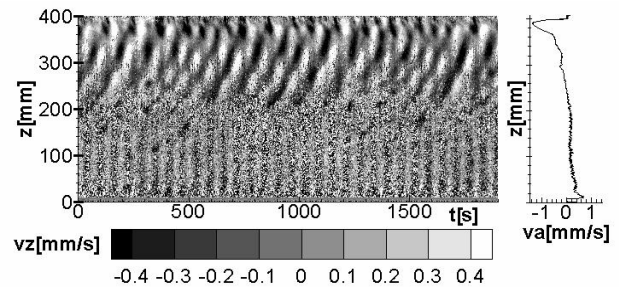
Figure 2: Raw data from one ultrasonic transducer with subtracted z-dependent time average velocity on the right.

The influence of the slight excentricity of the outer cylinder is clearly seen. This excentricity generates a shift of $180°$ between the two signals from outer rotation. To suppress this signal of the outer rotation we had to average both signals. Instead of doing this in time domain, we transformed both signals with standard FFT into frequency domain, like it is shown in figure 3a for one sensor. For each frequency the average of both signals is calculated. This Average of both channels is shown in figure 3b.
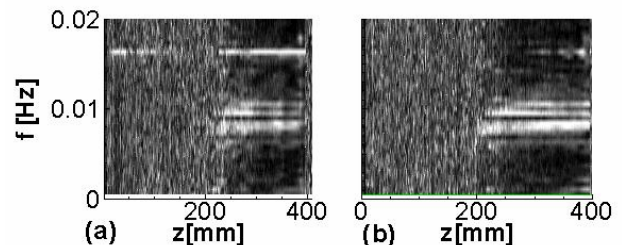
Figure 3: (a) Signal of one channel in frequency domain (b) Average of both channels, where outer rotation is suppressed.

In order to show this improvement (figure 4), we are using standard inverse FFT algorithm for the signal in figure 3b. The vertical stripes on the bottom of figure 2 are reduced, so the signal from outer rotation is suppressed. The quality of the signal can

be improved even more by taking into account, that MRI is expected only in a certain frequency range and a certain wave length, which could clearly be identified in figure 4. This improvement can be done by using a bandpass filter. As simplification we use only a low pass filter cutting off only high frequencies and the short wavelengths.
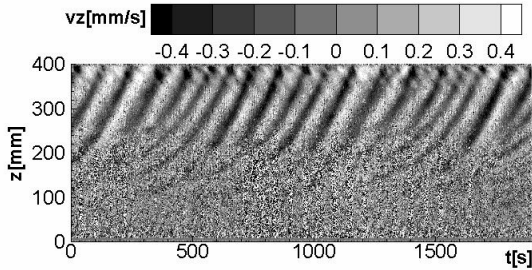
Figure 4: Average of both signals with suppressed signal from excentricity.

The low pass filtering is again done in frequency domain using the averaged signal shown in figure 3b. A very sharp filter characteristic is used by clearing all frequencies above $f_{LP} = 0.015 Hz$. Figure 5 shows the clearly improved signal after inverse FFT transformation, but the information about the typical MRI wavelength is not yet considered in post processing.
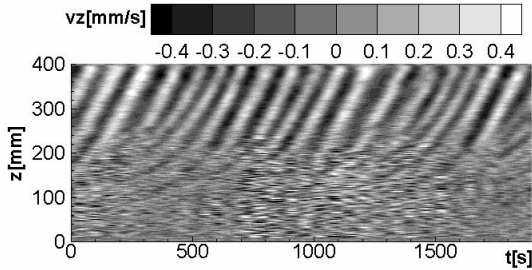
Figure 5: Signal after low pass filtering in frequency domain.

To implement this enhancement the signal is transformed with FFT into wave number domain. All waves with a wavelength below $\lambda_{LP} = 20 mm$ are suppressed by clearing all wave numbers ($k = 2\pi / \lambda$, thereby λ is the wavelength) above $k = 0.31 / mm$.
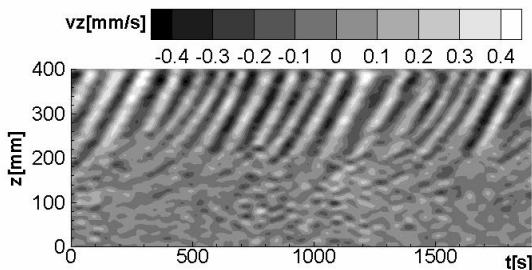
Figure 6: Signal after cutting off short wavelengths in wave number domain.

Figure 6 shows the result of the whole data processing using FFT. Similar results can be produced, by averaging the signal in time domain and using a 2D gauss filter in time domain, but consuming more computation time. The diagrams shown in the next paragraph are processed with the former described algorithm.

4. SOME RESULTS

We have carried out a large number of experimental runs in order to cover a wide range of parameter dependencies. Typically, the duration of an experimental run was 1900 sec, after a waiting time of one hour and more, depending on the distance to criticality and wave velocity. Many details for the first experimental campaign PROMISE 1 can be found in the publications [7-9].

Due to the reflection symmetry breaking under the influence of a helical magnetic field [11], the Taylor vortex flow is replaced by an oscillatory axi-symmetric vortex flow that propagates in a unique direction along the vertical axis [5,6]. This direction depends on the sign of the product of rotation direction, axial, and azimuthal magnetic field. The travelling wave appears already with a stationary outer cylinder, i.e. at $\mu := f_{out} / f_{in} = 0$, although with a very low frequency. With increasing μ, the wave frequency increases and typically reaches a value of $(0.1...0.2) \cdot f_{in}$ at the Rayleigh value $\mu_{Ray} := (r_{in} / r_{out})^2 = 0.25$. While μ_{Ray} would be a sharp boundary between unstable and stable flows in the purely hydrodynamic case, the interesting point is now that under the influence of helical magnetic fields the instability extends beyond $\mu_{Ray} = 0.25$ [6,9]. Typically, this shift of the boundary to higher values of μ becomes larger for increasing values of the ratio of azimuthal field to axial field, $\beta = B_\varphi (r = r_{in}) / B_z$.

One of the most significant features of the MRI is that, for fixed Re and fixed azimuthal field, it shows up only in a finite interval of the Hartmann number $Ha = B_z (r_{in} d\sigma / \rho\nu)^{1/2}$ (ρ is density, and ν is kinematic viscosity). This appearance and disappearance of a travelling mode is a suitable indicator for the existence of the proper MRI mode and its distinction from other possible flow structures. The results presented in figure 7 are for rotation rates of $f_{in} = 0.06 Hz$ and $f_{out} = 0.0162 Hz$, i.e. for $\mu = 0.27$ which is slightly above the Rayleigh value $\mu_{Ray} = 0.25$. Figure 7 documents a selection of four experimental runs for coil currents I_{coil} of 0, 50, 75 and 120 A. In the present PROMISE 2 case the axial current I_{rod} was fixed to 7000 A. The grey scale of the plots represents the axial velocity v_z

processed with the algorithm described in section 3 before.
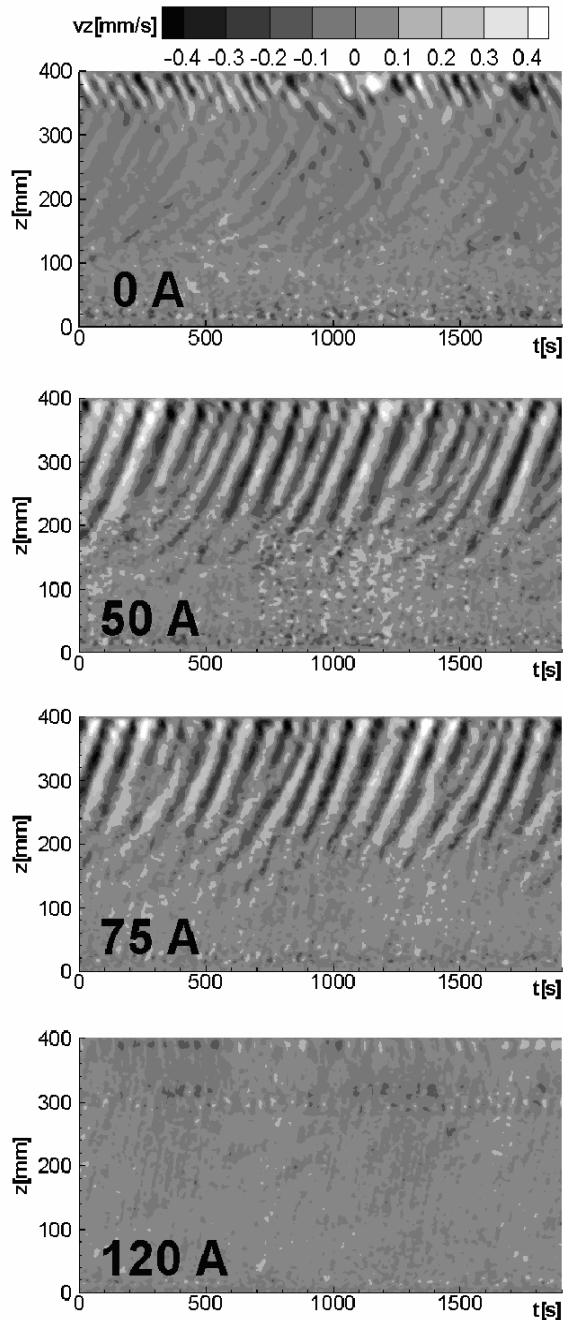
Figure 7. Axial velocity perturbation for differing coil currents during PROMISE 2 experiment at $f_{in} = 0.06\,\text{Hz}$ and $f_{out} = 0.0162\,\text{Hz}$, i.e. $\mu = 0.27$, $I_{rod} = 7000\,\text{A}$.

We observe the typical behaviour that MRI comes up in a finite interval of the coil current (which is proportional to the Hartmann number), the wave growth from the bottom and propagates throughout the total height of the cell. The upward growth of the amplitude is quite typical for an travelling wave instability like the helical MRI for which the absolute instability, in contrast to the convective one, is characterized by a complex wave number [12].

5. CONCLUSIONS

We have obtained experimental evidence for the existence of the MRI in helical magnetic fields, in particular by showing its appearance in a certain interval of the Hartmann number. The symmetrization of the axial boundary conditions and the use of split end caps in PROMISE 2 has lead to a strong reduction of the Ekman pumping and hence to a avoidance of artefacts in the radial jet flow region. We could enhance the quality of the visualisation by using standard FFT. Further dependencies of the MRI on parameters like μ, β, and Re, as well as their comparison with numerical predictions will be published elsewhere.

ACKNOWLEDGEMENT

REFERENCES

[1] Velikhov, E.P.: Stability of an ideally conducting liquid fluid between cylinders rotating in a magnetic field. Sov. Phys. JETP 9 (1959) 995-998

[2] Balbus, S.A.; Hawley, J.F.: A powerful local shear instability in weakly magnetized disks. 1. Linear Analysis. Astrophys. J. 376 (1991) 214-222

[3] Gailitis, A.; Lielausis, O.; Platacis, E.; Gerbeth, G., Stefani, F.: Laboratory experiments on hydromagnetic dynamos. Rev. Mod. Phys. 74 (2002) 973-990

[4] Rosner, R.; Rüdiger, G.; Bonanno, A. (Eds.): MHD Couette flows: Experiments and Models, AIP Conference Proceedings No. 733 (2004) New York: AIP

[5] Sisan, D. et al.: Experimental observation and characterization of the magnetorotational instability. Phys. Rev. Lett. 93 (2004) 114502

[6] Hollerbach, R.; Rüdiger, G.: New type of magnetorotational instability in cylindrical Taylor-Couette flow. Phys. Rev. Lett. 95 (2005) 124501

[7] Stefani, F. et al.: Experimental evidence for magnetorotational instability in a Taylor-Couette flow under the influence of a helical magnetic field. Phys. Rev. Lett. 97 (2006) 184502

[8] Rüdiger, G. et al.: The travelling-wave MRI in cylindrical Taylor-Couette flow: Comparing wavelengths and speeds in theory and experiment. Astrophys. J. Lett. 649 (2006) L145-L147

[9] Stefani, F. et al.: Experiments on the magnetorotational instability in helical magnetic fields. New J. Physics 9 (2007) 295

[10] Szklarski, J.: Reduction of boundary effects in spiral MRI experiment PROMISE. Astron. Nachr. 328 (2007) 499-506

[11] Knobloch, E.: Symmetry and instability in rotating hydrodynamic and magnetohydrodynamic flows. Phys. Fluids 8 (1996) 1446-1454

[12] Gerbeth, G; Priede, J.: Absolute vs. convective helical MRI in a TC flow. Presentation at the MRI workshop, Catania, 1-3 October 2007